Seeded optically driven avalanche ionization in molecular and noble gases

Pavel Polynkin,* Bernard Pasenhow, Nicholas Driscoll, Maik Scheller, Ewan M. Wright, and Jerome V. Moloney
College of Optical Sciences, The University of Arizona, Tucson, Arizona 85721, USA
(Received 15 August 2012; published 5 October 2012)

We report experimental and numerical results on the dual laser-pulse plasma excitation in molecular and noble gases at atmospheric pressure. Dilute plasma channels generated through filamentation of ultraintense femtosecond laser pulses in air, argon, and helium are densified through the application of multijoule nanosecond heater pulses. Plasma densification in molecular gases is always accompanied by the fragmentation of the plasma channels into discrete bubbles, while in atomic gases, under certain conditions, the densified channels remain smooth and continuous. The densification effect in atomic gases persists through considerably longer delays between the femtosecond and nanosecond pulses compared to that in molecular gases. Using rate equations we trace this difference in the temporal dynamics of densification to the different cooling mechanisms operative in atomic and molecular cases.

DOI: 10.1103/PhysRevA.86.043410 PACS number(s): 32.80.Rm, 33.80.Rv, 52.25.Jm, 34.80.Gs

I. INTRODUCTION

Experiments on ionization of gases by powerful laser pulses date back to the early 1960s [1]. Active studies in this field over the following two decades were primarily motivated by the potential use of laser-generated plasmas in controlled nuclear fusion. (For a review of the subject see, for example, [2].)

Q-switched solid-state lasers with pulse energies in the multijoule range and beyond and nanosecond-scale pulse durations are the laser sources that are commonly used in experiments on ionization of gaseous media. The physical mechanisms responsible for gas ionization by such lasers are well understood. When the intensity of the tightly focused laser beam exceeds a certain threshold level, an optically driven avalanche develops. Free electrons participating in the avalanche are accelerated by the intense laser field through the inverse bremsstrahlung process that involves their collision with neutral and already ionized molecules. Once the accelerating electrons attain energy that equals the ionization potential of neutral molecules, these electrons impact-ionize more molecules, forming an electron avalanche. The few seed electrons needed to start the avalanche are typically provided by multiphoton ionization of some impurity molecules with low ionization potential.

Ionization of gases by nanosecond (or longer) laser pulses is commonly referred to as optical breakdown, due to its similarities with electrostatic gas breakdown in the underlying physics. Being a thresholdlike process with respect to the intensity of the laser field, optical breakdown offers very limited means of control over plasma generation. For example, for clean, dust-free air, the breakdown intensity threshold is of the order of 10^{11} W/cm^2 [3]. In order to reach this intensity level in experiments on plasma generation in gases with nanosecond laser pulses, tightly focused experimental geometries are typically used. The plasma plumes generated under such conditions are dense, with nearly all gas molecules ionized, sometimes several times over. However, the longitudinal extent of these plasmas is limited by the Rayleigh range of the focusing optics and typically does not exceed several centimeters. (Note that the generation of extended plasma channels in air with the length of tens of meters has been demonstrated using one-of-a-kind ultraenergetic CO_2 and solid-state lasers with pulse energies of the order of 1 kJ [4,5].) Generally, the generation of extended plasma channels at ranges of hundreds of meters and beyond, as required by various remote sensing applications, poses fundamental challenges if nanosecond laser sources are used.

An alternative mechanism of plasma production in gases that has recently attracted significant attention is through femtosecond laser filamentation [6–8]. In femtosecond laser filaments, the dynamic balance between Kerr self-focusing, diffraction, and defocusing by plasma, produced on the beam axis via multiphoton ionization, results in the generation of extended plasma channels that can be many meters long. Laser filaments can be straightforwardly produced at standoff distances by using negatively chirped femtosecond laser pulses. As these chirped pulses propagate, the natural air dispersion dechirps them and the self-focusing collapse with the associated plasma channel generation occurs at a particular distance controlled by the value of the initial temporal chirp. Femtosecond laser filamentation provides for a significant degree of control over plasma generation at range. However, since plasma production is halted as soon as its defocusing action is sufficient to balance Kerr self-focusing, the density of plasma in femtosecond filaments is very low. Fewer than 1% of all molecules are ionized in femtosecond filaments under typical atmospheric conditions, which is one of the major factors limiting potential applications of laser filaments.

Proposals that suggest the combination of femtosecond and nanosecond plasma excitation mechanisms have been discussed for quite some time [9–11]. In the combined femtosecond-nanosecond (fs-ns) excitation approach, dilute seed plasma is generated through femtosecond laser filamentation. The seed plasma is subsequently heated and densified through avalanche ionization driven by a copropagating energetic nanosecond heater pulse. This approach combines the advantages of straightforward control over the longitudinal plasma channel placement that is offered by filamentation of prechirped femtosecond laser pulses, with the ability to generate dense plasmas through nanosecond optical breakdown. Potential applications of extended and

*ppolynkin@optics.arizona.edu

dense plasma channels generated through the application of this approach include guiding microwaves [12] and remote initiation of sources of backward-propagating laserlike light in the atmosphere [13].

The combined fs-ns plasma excitation approach has been recently demonstrated experimentally [14]. We will refer to this technique as to the igniter-heater excitation scheme, following the terminology used in the laser wakefield particle acceleration community, where this approach was originally proposed and investigated [15]. In the proof-of-principle experiments [14], dense plasma channels in air were generated through the joint application of copropagating 500 fs, 15 mJ igniter and 10 ns, 3 J heater pulses. The maximum length of the densified channels was about 10 cm. Although the plasma channels thus generated were dense, plasma densification was always accompanied by the channel fragmentation into discrete plasma bubbles. It has been pointed out that channel fragmentation into bubbles is an undesirable effect that limits potential application space for this approach. The exact physical mechanism responsible for the channel fragmentation remains unclear at this time.

In this paper, we report the extension of the original experiments [14] on dense plasma generation in air, which is a molecular gas, to the cases of the atomic gases argon and helium. In contrast to the case of a molecular gas, where the plasma channel densification is always accompanied by its fragmentation into discrete bubbles, in noble gases, under certain conditions, the densified cannels remain smooth and continuous. Furthermore, plasma densification in noble gases can be achieved for significantly longer delays between the femtosecond igniter and nanosecond heater pulses, compared to that in a molecular gas. A simple model based on the rate equations for the density and temperature of the electron gas, under the combined action of the femtosecond and nanosecond laser pulses, provides reasonable agreement with the experiment for the temporal dynamics of the densification. The model further points to the different electron cooling mechanisms in the atomic and molecular gases as the physical source of the different temporal dynamics of densification in the two cases.

II. EXPERIMENTAL SETUP

Our experimental setup is schematically shown in Fig. 1. Seed plasma filaments are produced through multiphoton ionization driven by weakly focused igniter laser pulses at 800 nm wavelength, with pulse energy of up to 15 mJ.

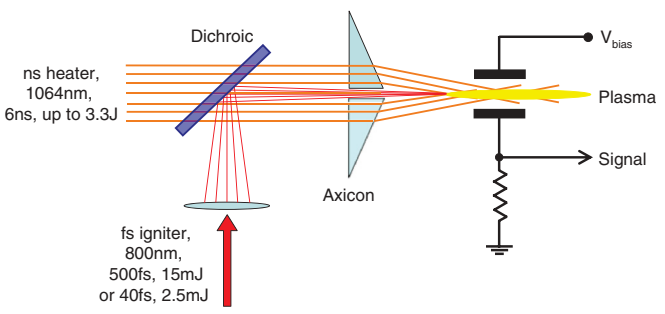

FIG. 1. (Color online) Experimental setup.

The igniter pulses are produced by a commercial chirped-pulse-amplification system that generates pulses with 30 nm optical bandwidth. Two kinds of igniter pulses are used: either temporally chirped pulses with 500 fs duration and pulse energy of up to 15 mJ, or fully compressed pulses with duration of about 40 fs and pulse energy of 2.5 mJ. In both cases, the peak power of the igniter pulses is chosen to remain below the onset of white-light generation and damage in the focusing optics. The input beam diameter of the igniter pulses is 5 mm, and the focal length of the lens used to focus the igniter beam is 50 cm. Under these conditions, the filamentation of the igniter results in the generation of an about 20-cm-long dilute seed plasma channel.

The igniter plasma is densified through the application of energetic heater pulses with about 6 ns pulse duration and up to 3.3 J of energy per pulse. The heater pulses are produced by an amplified Q-switched Nd:YAG laser operating at 1064 nm wavelength. Both igniter and heater lasers operate at 10 Hz pulse repetition frequency. The pulse trains from the two lasers are synchronized to within less than 0.5 ns, through a common triggering.

The heater beam is focused by a conical lens (axicon), with the apex angle of 175°, and spatially combined with the igniter beam via a dichroic beam combiner. The beams are aligned to overlap the 20-cm-long linear focus zone of the heater beam with the Rayleigh zone of the igniter. The axicon lens used to focus the heater has a 5-mm-diameter hole drilled through its center. The distance that the weakly focused igniter beam travels from the focusing lens to the axicon is about 15 cm. When the igniter beam reaches the axicon, its diameter is reduced to about 3.5 mm, so it passes through the hole in the axicon undisturbed on its way to the filamentation zone.

For experiments in argon and helium, the entire beam-combination setup, including the focusing lenses for the igniter and heater beams and the dichroic beam combiner, is enclosed in an airtight box with 1-mm-thick fused-silica input and output windows. The box is flooded with ultrahigh-purity gases under slightly positive pressure relative to the atmospheric pressure outside the box. The purity of the gases inside the box is monitored by measuring the oxygen concentration in the leftover air, using an oxygen sensor that has less than 0.1 vol % accuracy. The experiments in noble gases are performed when the reading from the sensor is at its lower accuracy limit, indicating that the purity of the gas inside the box is better than 99.9%.

Plasma density in the seed filament, as well as in the densified plasma channel, produced through the joint application of the igniter and heater pulses, is characterized, on a relative scale, by using the capacitive plasma probe described in detail elsewhere [16]. The probe has 5-cm-long electrodes that are charged to 100 V. The electrodes are placed symmetrically around the generated plasma channel, longitudinally in the middle of the channel, where plasma density, both in the seed filament and in the densified channel, is at a maximum. The distance between the probe electrodes is 1 cm. The signal output from this kind of plasma probe has been argued to be approximately linear with respect to the density of plasma in the channel, for a particular gas [17]. The scale factors for the probe in different gases are different and depend on the ionic mobilities in these gases. Consequently, the plasma density

measurements using our probe in different gases cannot be straightforwardly compared to each other.

III. MODEL

For the purpose of interpreting our experimental results we have performed rate-equation simulations to compute the density N_e and temperature T_e of the laser-generated electron gas under the combined action of the igniter and heater pulses. Our rate equations are of the level of detail that is commonly employed in the literature for describing femtosecond laser-induced plasma generation in gases [6], but with the caveat that we also need to account for electron heating due to the heater pulse as well as for the various sources of electron cooling that can arise on the time scale of our experiment. We have attempted as far as possible to keep the complexity of the rate equations to a minimum while retaining the key physics underlying the differences between the temporal dynamics of plasma densification in atomic and molecular gases. More detailed rate equations exist but are beyond the needs of the present paper [18,19].

To proceed we next summarize the simplifying assumptions involved in our model. We use a point model that ignores spatial variations of the plasma and field parameters. However, the seed plasma is initiated by an igniter pulse in the form of a femtosecond light filament whose properties may be inferred. In particular, the intensity of the igniter pulse in the filamentation zone is taken equal to the clamping intensity that has been measured previously, giving approximate peak intensity values of 5×10^{13} W/cm^2 for air [20] and 1.5×10^{14} W/cm^2 for argon [21]. The heater intensity in the interaction zone is estimated from the input beam parameters, assuming that the linear focusing of the heater beam by the axicon lens is the dominant beam-shaping mechanism for the heater. This procedure yields peak heater intensity of 2.4×10^{11} W/cm^2 at the maximum pulse energy of 3.3 J attainable from the heater laser. The simulation of the response of the plasma probe is based on the assumption that the signal returned by the probe is proportional to the time-integrated electron density from our point model. In common with the experimental plasma probe, our simulations yield information on the plasma densification on the arbitrary unit scale. In spite of the above simplifying assumptions our model captures the basic physical picture of the dual-pulse plasma excitation reasonably well and allows us to elucidate the qualitative difference in the temporal characteristics of the generated plasma between the cases of molecular and atomic gases.

The system of coupled rate equations in our model, for the case of argon, consists of equations for the electron and ion densities $N_{e,i}$ and electron and background temperatures $T_{e,b}$. Turning first to the electron density, the relevant rate equation is

$$\frac{dN_e}{dt} = \beta_n I^n(t)(N_0 - N_e) + \frac{\sigma_B}{E_g} I(t) + \nu(T_e) N_e (N_0 - N_e) - \frac{K_0}{T_e^{0.67}} N_e^2 - \frac{N_e}{\tau} - \frac{1}{D}\sqrt{\frac{k_B T_e}{m_e}} N_e, \quad (1)$$

where $I(t)$ is the total intensity of the laser field composed of the femtosecond igniter and nanosecond heater components, and N_0 is the initial number density of neutral atoms. The first line in (1) describes electron generation via multiphoton ionization with the rate constant β_n. Multiphoton ionization is negligible during the lower-intensity heater pulse; thus, for the case of argon excited by the intense igniter pulse at 800 nm wavelength, $n = 11$. For argon and peak intensities of order 10^{14} W/cm^2 the Keldysh parameter is much less than unity so that the multiphoton ionization model is applicable [22]. The second line in (1) consists of two additive terms and describes impact ionization in two different temperature regimes. The first term proportional to σ_B, which is the cross section for ionization via inverse bremsstrahlung in the simple Drude-like model, dominates when electron temperature is below $\sim 10^4$ K. E_g is the ionization energy. For higher temperature, the second term proportional to $\nu(T_e)$ dominates. It accounts for the impact ionization of neutral atoms through their collisions with electrons occupying the high-energy tail of the thermal electron distribution with temperature T_e [23]. The third line of (1) describes electron losses from the generated plasma string: The first term describes recombination and accounts for both direct and dissociative recombination channels, the second term accounts for losses due to electron attachment, and the third term accounts for diffusion of electrons out of the plasma string with the approximate diameter of $D = 50$ μm. Particularly relevant for the ensuing discussion is the fact that the electron recombination term varies inversely with the electron temperature to the power of 0.67 [24], so that a hotter plasma will survive longer, although it may also diffuse faster.

Next we turn to the rate equation for the electron temperature for the case of argon:

$$\frac{dT_e}{dt} = \frac{2e^2}{3k_B c\,\varepsilon_0 m_e \omega_0^2} \nu_e(T_e) I(t) - \frac{2m_e}{m_n} f_e(T_e)(T_e - T_b) - \left(T_e + \frac{2E_g}{3k_B}\right) \frac{1}{N_e} \left[\frac{dN_e}{dt}\right]_{ion}, \quad (2)$$

where T_b is the background temperature of ions and neutrals [25]. Here the first line on the right-hand side describes heating of the electron gas by the igniter and heater pulses, the second line describes the effect of electron-ion and electron-neutral collisions with the effective scattering rate $f_e(T_e)$, and m_n is the mass of the neutral atom. The last line accounts for electron cooling due to the second ionization-related term appearing in the second line of (1). For the case of atomic gases such as argon, this cooling channel dominates over the other cooling mechanisms on the time scale of our experiment.

Rate equations of similar structure to (1) and (2) are employed for the case of air with some key differences that we now point out. The densities of the oxygen and nitrogen constituents of air are described by separate rate equations. The peak intensities of 5×10^{13} W/cm^2 are indicative of the tunneling regime of ionization as opposed to the multiphoton ionization model employed in Eq. (1). However, it is known that using noninteger values of multiphoton order n for oxygen and nitrogen allows one to straddle the multiphoton and tunneling regimes for intensities up to around 10^{14} W/cm^2 [26], and we have adopted that approach here. Additional rate equations are introduced for the density of the negative molecular oxygen ions formed through the attachment process of the liberated electrons to the neutral oxygen molecules.

These rate equations are well documented for femtosecond laser excitation [6] so here we do not expand upon this further. The key difference for the time scale of our experiment is that a new term must be added to the electron temperature rate equation (2) that describes relaxation of the electron temperature due to the energy transfer to the vibrational degrees of freedom of the molecules. The treatment of the extra vibrational term is described in detail for the case of air by Sun *et al.* [25], and we have adopted their model here. A key observation is that the vibrational term limits the peak electron temperature in air to about 10 000 K, so that ionization in the electron density equation (1) is well described by the Drude term alone. The temperature dependence of recombination, for both oxygen and nitrogen constituents, is replaced by the $1/\sqrt{T_e}$ dependence [27]. Since the electron temperature is constrained in air, the recombination terms in the ionic density rate equations in this case are more prevalent. As a result, plasmas tend to recombine quicker in air than in argon.

We have solved the rate equations for air and argon for a range of temporal delays between the igniter and heater pulses. Our findings are presented in the next section. The various rate terms and numerical values of the rate constants for the densities and temperatures of the species involved were collected from the open literature [18,19,25]. We confined our simulations to the cases of air and argon as examples of molecular and atomic gases, respectively, since for the case of helium, the peak power of the igniter pulse attainable in the experiments was below the critical power for self-focusing. In that case, our approach for estimating the peak intensity of the femtosecond igniter pulse in the interaction zone, based on the intensity clamping argument, was not valid.

IV. RESULTS AND DISCUSSION

In our experiments, the plasma channels generated through igniter-heater excitation were photographed and their density was measured, on a relative scale, using the capacitive plasma probe described above. As also noted above, the experiments on plasma production were conducted using two kinds of femtosecond igniter pulses: 15 mJ pulses temporally chirped to about 500 fs duration and 2.5 mJ pulses compressed to sub-40 fs duration. The use of fully compressed igniter pulses with higher energy was precluded by the onset of white-light generation in the focusing optics for the igniter.

Qualitatively, for the case of air, the application of the lower-energy, fully compressed igniter pulses, together with the nanosecond heater pulses at their maximum available energy of 3.3 J, did not result in any measurable plasma. In our focusing geometry, the 3.3 J energy of the heater corresponds to about 2.4×10^{11} W/cm^2 of the heater peak intensity in the interaction zone. When 15 mJ, 500 fs chirped igniter was applied and the temporal delay between the igniter and heater pulses was optimized, plasma densification by the heater pulse was observed for heater pulse energies above ~2 J. The densified plasma channels in air were always fragmented into discrete plasma bubbles positioned randomly along the channel, with the average separation between the bubbles of about 0.5 mm. These observations are in line with those in the proof-of-principle demonstration [14].

For the case of argon, both 2.5 mJ compressed and 15 mJ chirped igniter pulses were sufficiently intense for the reliable seeding of the optical avalanche driven by the heater pulse. The densified plasma channels seeded by the longer pulse were fragmented into bubbles which were larger and more loosely spaced compared to the case of air. The densified channels seeded by the lower-energy compressed pulses remained continuous, as long as the peak intensity of the heater pulse was below 6×10^{10} W/cm^2.

To compare our experimental results with modeling, we selected the cases of air and argon, with seeding by the 15 mJ, 500 fs chirped igniter pulses in both cases. For the case of argon, the application of the heater pulse alone (without the igniter) resulted in the unseeded optical breakdown, when the heater intensity exceeded 1.5×10^{11} W/cm^2. Accordingly, the experiments in argon were conducted at heater intensities not exceeding that level, so that the optical breakdown driven by the heater pulse was always seeded by the igniter filament. Photographs of the seed plasma channel created through filamentation of the 15 mJ, 500 fs igniter pulse, as well as of the densified channel generated by the application of the igniter and heater pulses together, are shown, for the cases of air and argon, in Fig. 2. The estimated maximum intensity of the nanosecond heater pulse in the interaction zone corresponding to the cases shown is 2.4×10^{11} W/cm^2 in air and 1.4×10^{11} W/cm^2 in argon.

To investigate the temporal characteristics of plasma produced through the joint application of the femtosecond igniter and nanosecond heater pulses and to elucidate the qualitative difference between the cases of plasma excitation in molecular and atomic gases, we studied the dependence of the generated plasma density in air and argon, under similar excitation

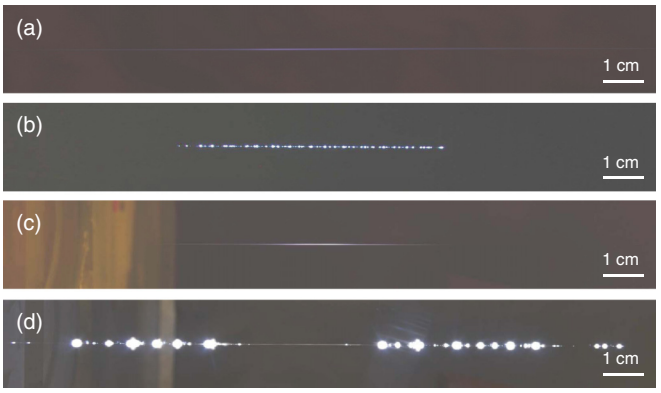

FIG. 2. (Color online) Photographs of the seed filaments and densified plasma channels in air (two top panels) and argon (two bottom panels). 500-fs-long, 15 mJ pulses are used for the generation of seed filaments in both cases. The delays between the femtosecond igniter and nanosecond heater pulses are optimized to maximize plasma production. The estimated peak power of the nanosecond heater pulse is 2.4×10^{11} W/cm^2 in air and 1.4×10^{11} W/cm^2 in argon. The heater intensity in both cases is below the threshold for unseeded optical breakdown. The photographs of the seed filaments in air (a) and argon (c) are averaged over 100 laser shots, in order to make faint seed plasma visible on the images. Photographs of the densified channels in air (b) and argon (d) are single shot. Under the excitation conditions used, the densified plasma channels are fragmented into bubbles in both gases. Plasma bubbles in argon are larger and more sparsely spaced compared to those in air.

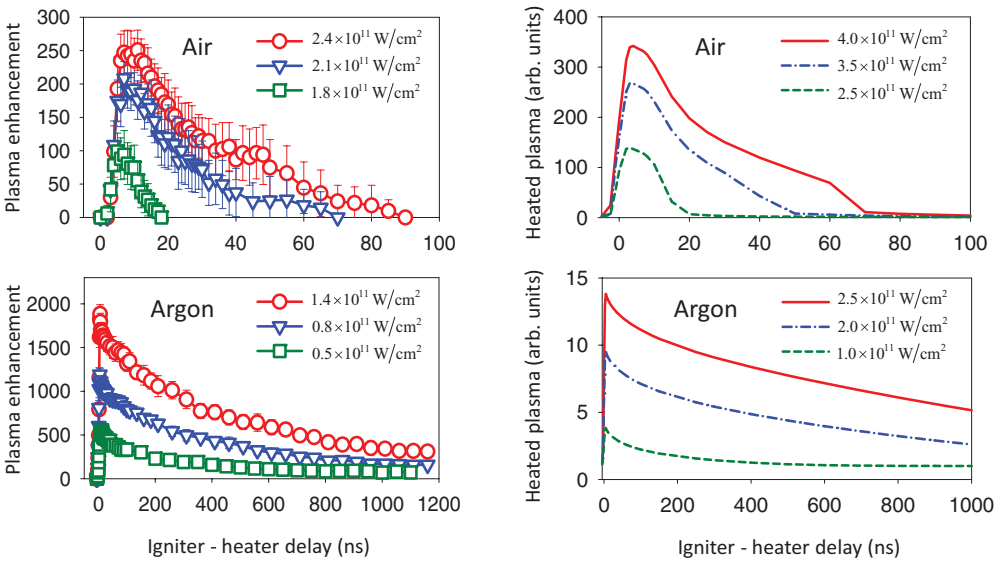

FIG. 3. (Color online) Time-integrated plasma density relative to that in the seed filament, vs delay between the femtosecond and nanosecond pulses in air and argon. The data are taken for several values of the on-axis intensity of the nanosecond pulse, as indicated in the legends. 500-fs-long, 15 mJ igniter pulses are used in both cases. Left column: experimental results. Right column: corresponding numerical simulations.

conditions, on the temporal delay between the igniter and heater pulses. The results are summarized in Fig. 3. Each data point is a result of averaging over 100 laser shots. From both experimental data and numerical simulations it is evident that in the case of air, the effect persists over the igniter-heater delay range of the order of several tens of nanoseconds, and that the value of the maximum igniter-heater delay at which the heating effect remains observable increases with the energy of the heater pulse. In the case of argon, the effect persists over a considerably longer range of igniter-heater delays of the order of 1 ms and beyond.

The above qualitative difference between the cases of molecular and atomic gases is attributed to the temperature dependence of the recombination rates in these gases. In air, seed electrons generated by the femtosecond igniter pulse are quickly cooled through the interaction with the molecular vibrational degree of freedom. Cool electrons quickly recombine with ions and become unavailable to seed the avalanche driven by the lagging heater pulse. In contrast, in argon, the vibrational damping is absent and seed electrons stay hot for a considerably longer time. Consequently, they recombine with parent ions much more slowly and enable the

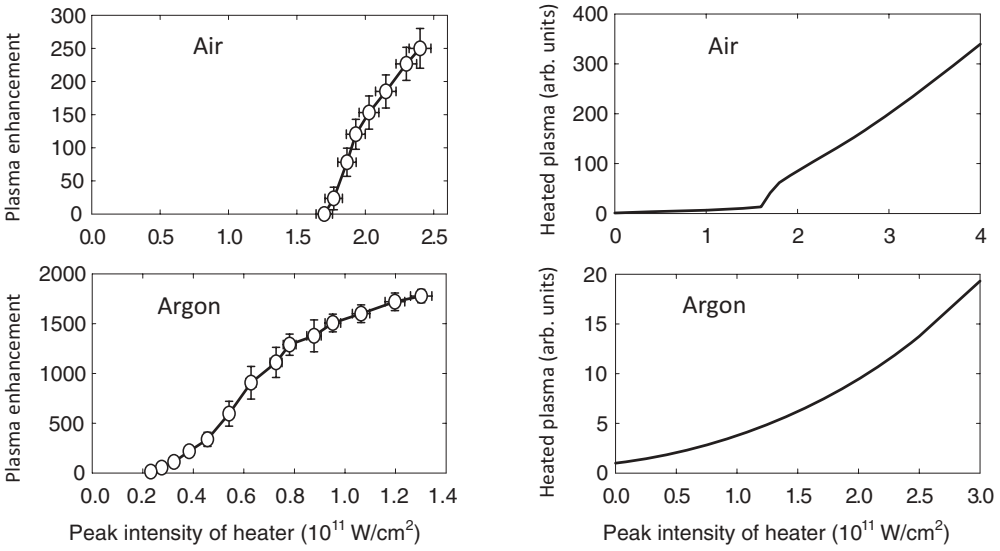

FIG. 4. Time-integrated plasma density relative to that in the seed filament, vs estimated on-axis intensity of the nanosecond heater pulses for air and argon. 500-fs-long 15 mJ igniter pulses are used in both cases. The delay between the femtosecond and nanosecond pulses is optimized to maximize plasma production at the maximum intensity level of the nanosecond pulse. Left column: experimental results. Right column: corresponding numerical simulations.

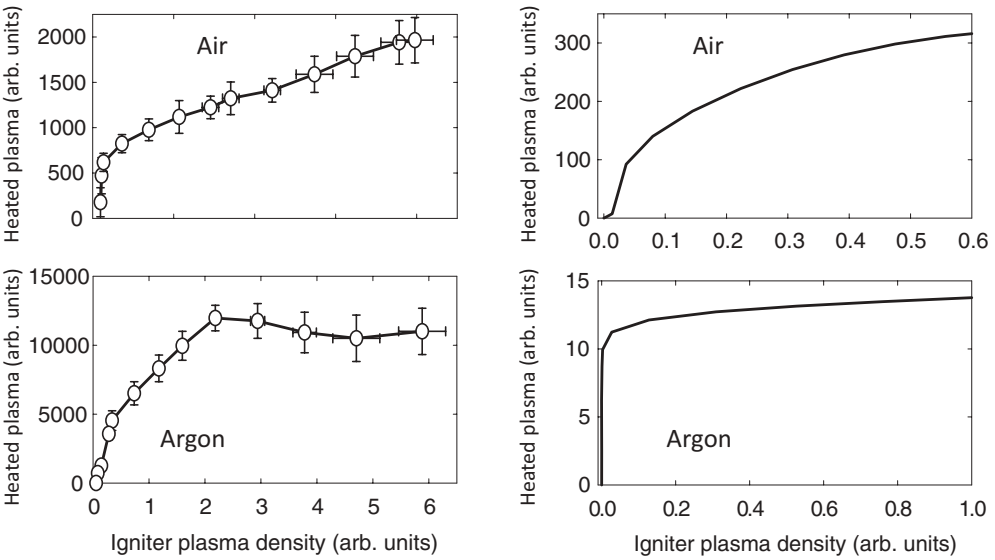

FIG. 5. Time-integrated plasma density, plotted on an arbitrary-unit scale, vs plasma density in the seed filament. The plasma density in the seed filament and in the densified plasma channel are plotted in the same arbitrary units, which are different in the cases of air and argon. The estimated on-axis intensity of the nanosecond heater pulse is 2.4×10^{11} W/cm^2 in air and 1.4×10^{11} W/cm^2 in argon. The delay between the femtosecond and nanosecond pulses is optimized to maximize plasma production at the maximum value of the seed plasma density. Left column: experimental results. Right column: corresponding numerical simulations.

seeded heater-driven avalanche breakdown for significantly longer igniter-heater delays.

In Fig. 4, we show the dependence of the electron density on the peak on-axis intensity of the heater pulse, at the optimum igniter-heater delay. On the nanosecond time scale, the optimum delay is of the order of the half-width of the heater pulse. As in Fig. 3 above, each data point is a result of averaging over 100 laser shots. The threshold response with respect to the heater intensity is evident in the cases of both molecular and atomic gases, although in the case of air the threshold is sharper. This qualitative trend is reproduced by numerical simulations based on the simple point model discussed above.

Examples of the dependence of the generated plasma density on the plasma density in the seed filament are shown in Fig. 5. The seed plasma produced through filamentation of the igniter pulse alone is characterized by the same capacitive probe that is used for the measurement of the densified plasma generated through the joint application of the igniter and heater pulses. The results of these measurements are qualitatively similar in the cases of molecular and atomic gases. The measured dependence involves a quick growth as the density of seed plasma is slightly increased above zero, after which the signal growth rate becomes more gradual. These trends are captured by the numerical simulations.

We point out again that a direct quantitative comparison between plasma yields in air and argon, based on the measurements with the capacitive plasma probe, is not possible. In the case of air, the probe does not collect and measure the generated electrons directly, but instead collects small residual amounts of positive and negative molecular ions. In the case of argon, where recombination of ions and hot electrons is much slower and the electron loss channel associated with their attachment to neutral atoms is not available, both free electrons and ions contribute to the measured signal. Furthermore, the agreement between our experimental results and numerical simulations is only qualitative. The dominant reasons for the lack of quantitative agreement are the inherent limitation of our point model that completely ignores the propagation effects for the heater pulse and uses a linear estimation for the heater intensity in the interaction zone and the unknown scale factor of the capacitive plasma probe which depends on the temperatures of the electronic and ionic subsystems.

The above experiments and numerical simulations utilized 15 mJ, 500 fs chirped igniter pulses and joule-level, 6 ns heater pulses, in both cases of air and argon. Additional observations of the igniter-heater plasma excitation were carried out for shorter and lower-energy igniter pulses in argon, as well as for both compressed and chirped igniter pulses in helium. In the case of argon, the energy of the heater pulses was kept below the level at which the heater beam alone was capable of initiating the unseeded gas breakdown. Photographs of the seed and densified plasma channels for two particular cases are shown in Fig. 6. For the case of argon excited by 2.5 mJ, 40-fs-long igniter pulses, we observed smooth and continuous densified plasma channels, as long as the peak intensity of the heater pulses in the interaction zone remained below 6×10^{10} W/cm^2. For the case of helium, both 2.5 mJ, 40 fs and 15 mJ, 500 fs igniter pulses had peak power below the power threshold for self-focusing. Notwithstanding that, seed plasma was still generated in both of those cases, because the igniter intensity in the interaction zone was made sufficient for ionization by the external focusing with a lens. In the case of helium, the densified plasma channels remained smooth and continuous over the entire range of our experimental parameters, including the highest attainable peak intensity of the heater beam of 2.4×10^{11} W/cm^2. The fact that we were

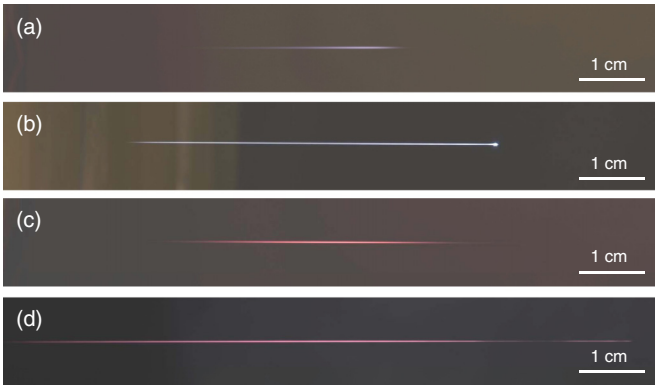

FIG. 6. (Color online) Photographs of the seed filaments and smooth densified plasma channels in argon (two top panels) and helium (two bottom panels). A 40-fs-long, 1.5 mJ igniter pulse is used in the case of argon. The photograph of the seed filament in this case is integrated over 300 laser shots (a). The densified plasma channel in argon remains smooth and continuous as long as the intensity of the nanosecond heater pulse remains under 6×10^{10} W/cm^2 (b). This image is integrated over ten laser shots. In the case of helium, the densified channel is smooth over the entire range of parameters of the igniter and heater pulses attainable in our experimental setup. For example, the dilute seed filament generated by 500-fs-long, 15 mJ igniter pulse in helium is shown in (c). This image is integrated over 100 laser shots. A single-shot image of the channel that is densified through the application of the nanosecond heater pulse with the peak intensity of 2.4×10^{11} W/cm^2 is shown in (d).

never able to produce such smooth channels in molecular gases such as air and nitrogen suggests that the fragmentation of the plasma channel may be in some way related to the molecular structure of the propagation medium. At this point, we cannot offer a plausible explanation for the fragmentation effect.

The temporal characteristics and power dependence of the dual-pulse plasma excitation in helium were found to be similar to those in argon. Plasma densification persisted well into the multimicrosecond range of delays between the femtosecond and nanosecond pulses, exhibited a smooth threshold with respect to the heater intensity in the interaction zone, and had a qualitatively similar dependence on the density of the seed plasma to that in the case of argon.

V. SUMMARY AND CONCLUSIONS

We conducted experiments on the densification of dilute plasma filaments generated through self-focusing of femtosecond igniter laser pulses, by copropagating joule-level heater laser pulses with the pulse duration in the several nanoseconds range. The experiments were carried out in air, argon, and helium. In air, plasma densification and heating was found to be always accompanied by plasma-channel fragmentation into discrete bubbles placed randomly along the channel and separated by the characteristic distance of about 0.5 mm. In noble gases, under certain conditions, the heated and densified channels remained smooth and continuous. Our observations suggest that the fragmentation of the channel into bubbles may be related to the molecular structure of the propagation medium, although the exact mechanism responsible for this effect has not been yet identified. We devised a simple model based on the rate equations for densities and temperatures of the electronic, ionic, and molecular species involved. In spite of the simplicity of the model, it adequately captured the basic features of plasma generation through the igniter-heater excitation in air and argon.

ACKNOWLEDGMENTS

This work was supported by the United States Air Force Office of Scientific Research under Contracts No. FA9550-10-1-0561 and No. FA9550-10-1-0237.

[1] R. Meyerand and A. Haught, Phys. Rev. Lett. **11**, 401 (1963).
[2] *Principles of Laser Plasmas*, edited by G. Bekefi (Wiley, New York, 1976).
[3] D. Lencioni, Appl. Phys. Lett. **25**, 15 (1974).
[4] V. V. Apollonov, L. M. Vasilyak, S. Yu. Kazantsev, I. G. Kononov, D. N. Polyakov, A. V. Saifulin, and K. N. Firsov, Quantum Electron. **32**, 115 (2002).
[5] V. A. Parfenov, L. N. Pakhomov, V. Yu. Petrun'kin, and V. A. Podlevski, Pis'ma v Zhurnal Tekhnicheskoi Fiziki **2**, 731 (1976) [Sov. Tech. Phys. Lett. **2**, 286 (1977)].
[6] A. Couairon and A. Mysyrowicz, Phys. Rep. **441**, 47 (2007).
[7] L. Berge *et al.*, Rep. Prog. Phys. **70**, 1633 (2007).
[8] S. L. Chin, *Femtosecond Laser Filamentation* (Springer, Berlin, 2010).
[9] Z. Henis, G. Milikh, K. Papadopoulos, and A. Zigler, J. Appl. Phys. **103**, 103111 (2008).
[10] M. N. Shneider, A. N. Zheltikov, and R. B. Miles, Phys. Plasmas **18**, 063509 (2011).
[11] P. Sprangle, J. Peñano, B. Hafizi, D. Gordon, and M. Scully, Appl. Phys. Lett. **98**, 211102 (2011).
[12] V. D. Zvorykin, A. O. Levchenko, A. V. Shutov, E. V. Solomina, N. N. Ustinovskii, and I. V. Smetanin, Phys. Plasmas **19**, 033509 (2012).
[13] P. R. Hemmer, R. B. Miles, P. Polynkin, T. Siebert, A. V. Sokolov, P. Sprangle, and M. O. Scully, Proc. Natl. Acad. Sci. USA **108**, 3130 (2011).
[14] P. Polynkin and J. V. Moloney, Appl. Phys. Lett. **99**, 151103 (2001).
[15] P. Volbeyn, E. Esarey, and W. Lemans, Phys. Plasmas **6**, 2269 (1999).
[16] P. Polynkin, M. Kolesik, A. Roberts, D. Faccio, P. Di Trapani, and J. V. Moloney, Opt. Express **16**, 15733 (2008).
[17] D. Abdollahpour, S. Suntsov, D. G. Papazoglou, and S. Tzortzakis, Opt. Express **19**, 16866 (2011).
[18] A. Kossyi, A. Yu. Kostinsky, A. A. Matveev, and V. P. Silakov, Plasma Sources Sci. Technol. **1**, 207 (1992).

[19] A. Bogaerts and R. Gijbels, J. Appl. Phys. **86**, 4124 (1999).
[20] A. Becker, N. Akozbek, K. Vijayalakshmi, E. Oral, C. M. Bowden, and S. L. Chin, Appl. Phys. B: Lasers Opt. **73**, 287 (2001).
[21] S. Xu, J. Bernhardt, M. Sharifi, W. Liu, and S. L. Chin, Laser Phys. **22**, 195 (2012).
[22] L. V. Keldysh, J. Exper. Theor. Phys. **47**, 1945 (1964) [Sov. Phys. JETP **20**, 1307 (1965)].
[23] D. A. Romanov, R. Compton, A. Filin, and R. J. Levis, Phys. Rev. A **81**, 033403 (2010).
[24] F. J. Mehr and M. A. Biondi, Phys. Rev. **176**, 322 (1968).
[25] Z. Sun, J. Chen, and W. Rudolph, Phys. Rev. E **83**, 046408 (2011).
[26] J. Kasparain, R. Sauerbrey, and S. L. Chin, Appl. Phys. B: Lasers Opt. **71**, 877 (2000).
[27] P. M. Mul and J. W. McGowan, J. Phys. B **12**, 1591 (1979).